NG-DPSM: A Neural Green-Distributed Point Source Method for Modelling Ultrasonic Field Emission Near Fluid-Solid Interface using Physics Informed Neural Network

Ayush Thakur[1], Nur M. M. Kalimullah[1], Amit Shelke[1*], Budhaditya Hazra[1], Tribikram Kundu[2]

[1]Department of Civil Engineering, Indian Institute of Technology Guwahati, Assam 781039, India

[2]Department of Civil & Architecture Engineering & Mechanics, University of Arizona, Tucson, AZ 85721, USA

*Email: amitsh@iitg.ac.in

Abstract

Distributed point source method (DPSM) is a collocation point-based semi-analytical method to model the scattered ultrasonic fields in isotropic and anisotropic materials. It requires the evaluation of Green's function solutions and its rigorous differentiation for complex geometry problems having a large set of distributed point sources. DPSM is much faster than the finite element method (FEM) however, it is analytically demanding as it requires differentiation of the Green's function. The intricacy associated with differentiation operation hinders the potential application of DPSM in large-scale automation and real-time structural health monitoring. The current paper introduces machine-learning-based strategies within DPSM and yields the proposed Neural Green-DPSM (NG-DPSM) framework. A physics-informed neural network (PINN) is incorporated in the DPSM framework for evaluating the Green's function and its gradients. To train the PINN, displacement Green's function solutions of wave propagation in isotropic solid is used as the governing physics. Once the PINN is trained for displacement Green's function solutions, the NG-DPSM framework leverages the trained network and its automatic differentiation capability to predict displacement and stress fields annihilating the rigorous differentiation of Green's functions. The accuracy and efficacy of NG-DPSM are demonstrated using two numerical experiments. First, the ultrasonic fields are evaluated for the problem geometry of a plate immersed in fluid excited at different angles of incidence. Further, the efficacy of the proposed approach is demonstrated for wave scattering through a circular hole in the plate. The results show a strong agreement between the ultrasonic fields computed using both NG-DPSM and conventional DPSM.

Keywords: deep learning, DPSM, Green's function, isotropic material, physics informed neural network

1. Introduction

The non-destructive testing (NDT) is an essential step for structural health monitoring (SHM). Ultrasonic waves can be used for the non-destructive evaluation (NDE) of metals, composites, and other materials. The ultrasonic signals are transmitted and then received by placing sensors to detect flaws in the structures non-destructively [1, 2]. Various numerical schemes have been developed for the evaluation of ultrasonic signals to detect anomalies and have gained lots of traction in the domain of NDE. The application of distributed point source method (DPSM) has been prevalent in addressing ultrasonic and electromagnetic field modelling problems, particularly focusing on NDE purposes. In practical scenarios, the problem geometry often involves both fluid and solid mediums. It is common to immerse the solid specimen in a fluid medium for inspection, especially in the NDT of solid materials. This fluid acts as an effective coupling medium for ultrasonic waves. The ultrasonic waves propagate from the transducer to the solid specimen through this coupling fluid. Consequently, in real-world applications, it is essential to accurately model the acoustic beams and fluid-solid interfaces. DPSM has been successfully applied in modelling complex problem geometries such as wave propagation in multilayered fluid and solid structures [3, 4], solid plates both with and without cavities [5, 6], as well as in corrugated plates submerged in fluid [7, 8]. Additionally, DPSM has been instrumental in modelling half spaces containing multiple cavities [9] and in the modelling of acoustic microscope lenses for the characterization of biological cells [10].

DPSM is a semi-analytical technique used efficiently to compute ultrasonic fields in solids and fluids using a set of source and target points [5, 11]. Green's function is the main constituent of DPSM as it provides the fundamental relation between a pair of source and target points. The superposition of Green's function solution for different pairs of source and target points corresponds to the formulation of the DPSM technique for isotropic and anisotropic materials. Ultrasonic fields are calculated for multiple pairs of source and target points in the fluid and solid using the source strength matrix. A global system of equations can be formed for fluid-solid interface after applying the boundary constraints. The source strength is computed by solving a system of equations using the matrix inversion technique. The displacement, pressure, velocity, and stress fields are evaluated at any arbitrary point by superposing the effect of different source points at a target point using the source strength matrix. In the present work, a novel deep learning (DL) approach is proposed to estimate scattered ultrasonic fields near fluid-solid interfaces.

Several methods are available in the literature for modelling ultrasonic wave propagation in solids and fluids, for instance, the finite difference method (FDM) and finite element method (FEM) are the two most popular numerical techniques. In these methods, the ultrasonic fields are computed by solving the governing differential equation in a discretised domain of the problem geometry. The computational complexity arises in meshing the large three-dimensional (3D) domain while modelling of waves scattered by cracks and inclusions and the use of absorbing boundaries.

To cater above mentioned challenges, DPSM was developed to solve various scientific and engineering problems such as electrostatic, electromagnetic, and ultrasonic wave propagation problems [12, 13]. Since its inception, DPSM was established for solving ultrasonic wave propagation problems for solid-fluid interaction and layered mediums in isotropic materials [4, 14]. Banerjee *et al* employed DPSM to calculate elastic wave fields in multi-layered nonplanar solid structures [4]. Further, it is extended to model scattered wave fields in a solid half-space having internal anomalies such as a circular hole or an elliptical cavity [6, 15]. Recently, Fooladi and Kundu expanded the DPSM formulation to anisotropic materials [11, 16]. Since, no closed form expression for Green's function is available in the literature the elastodynamic Green's function for anisotropic materials it is evaluated numerically. In case of transversely isotropic materials for computing Green's function Fooladi and Kundu reduced the integration domain for the regular part of the solution from a hemisphere to a quarter-hemisphere. The suitability of DPSM in various problem domains has demonstrated itself as a superior technique in comparison to FEM in terms of computational time [12, 17]. For instance, the study carried out by Jarvis and Cegla compared DPSM and FEM for calculation of ultrasonic wave reflection through a rough surface and concluded that, FEM solution is slower than the equivalent DPSM simulation by two orders of magnitude, performed on the same machine [17].

The DPSM model is constructed using Green's function solutions which act as the building block for the propagation of ultrasonic waves through isotropic and anisotropic materials, and along the fluid-solid interface. Since, DPSM is a collocation point based approach, different sets of Green's functions for a sufficiently large number of source and target point pairs are evaluated resulting in large computational time, especially if the analytical solution of Green's function is not available. Fooladi and Kundu proposed a method called "windowing" that significantly lowered the number of Green's function evaluations [11, 16]. Further, in order to establish a suitable balance between computation time and accuracy, numerical integration using multiple resolutions was performed for computing Green's function

corresponding to various coordinates for transversely isotropic materials. Although the conventional DPSM technique is revised to make it computationally efficient, however, calculating Green's function solutions at every point still requires rigorous algebraic calculations pertaining to heavy reliability on the computing power. Moreover, the evaluation of stress fields requires the calculation of the gradient function for each of displacement Green's function solutions, which additionally increases computational complexity. To address these issues, in the present work, a physics-based DL methodology is adopted to estimate the ultrasonic fields using DPSM. It is worth mentioning that to the best of our knowledge, this work is the first implementation of DL architecture within the DPSM framework to model ultrasonic fields.

Machine learning (ML) and artificial intelligence (AI) have shown their great capability for solving many engineering problems and offer various possibilities to innovate the domain of SHM using data-driven modelling. The combination of ML, big-data and AI has gained a lot of recognition in science and engineering [18-21]. Neural networks (NNs) being universal function approximator [22, 23] can handle any arbitrary function having large number of dimensions. Artificial NN (ANN) uses a feed-forward network that can be used to solve partial differential equations (PDEs) and algebraic equations. The network is trained using large amount of data for the accuracy of the model. Even where the governing physical laws of the system are well known, researchers are more inclined towards the data-driven approach, which leads to additional data curing. ANN based data-driven modelling has been implemented for ultrasonic wave propagation [24] and acoustic emission (AE) source localisation [25, 26] in complex systems. Raissi*, et al.* first used a physics induced DL approach to solve non-linear PDEs using the governing physical laws and the boundary constraint of the problem [27]. The NN approximates underlying physics and boundary constraints using a set of nonlinear operators. The PINN is trained by minimising the loss function consisting of physics loss, initial and boundary condition losses, and other physical constraint losses. Further, the learnable parameters of the network, i.e., the weights and biases are trained to give approximate solutions for the nonlinear system of equations. Since its conceptualization, PINN is well established to solve forward problems in the field of quantum mechanics such as the non-linear Schrodinger equation having periodic boundary conditions using both continuous and discrete-time models. Raissi, *et al.* utilise PINN as an inverse problem for the parameter estimation of PDE by calculating the pressure and velocity field for 2D Navier-Stokes equation in case of incompressible fluid flow using noisy data. In addition to solving PDEs, PINN has been applied

in the field of fracture mechanics, dynamical systems, and continuum mechanics [28-31]. Shukla, *et al.* identified cracks in a metal by training PINN for non-destructive evaluation of surface breaking cracks [31]. The acoustic wave equation of second order is utilised in this study for modelling wave propagation in the temporal domain. Wang, *et al.* modelled the scattered acoustic field in a 2d plate using PINN [32]. Ultrasonic waves in various media are propagated using standard acoustic wave equation and the model is trained for scattered wave fields in case of real and complex damaged structures. With the further advancement in the PINN's theory and the development of Deep-O-nets [33], DL has been successful in learning Green's function which serves as a powerful tool in solving differential equations. Recently, Lin, *et al.* developed a novel boundary integral equation-based GreenNet method (BI-GreenNet) for computing Green's function for Poisson and Helmholtz equations in bounded and unbounded domains [34]. Zhang, *et al.* proposed a model-operator-data network (MOD-Net) to solve PDEs using the Green's function. The deep NN is used to parameterize the Green's function and the neural operator is obtained to compute the solution using Green's function [35].

In this paper, a Neural Green-DPSM (NG-DPSM) framework based on PINN is developed. The NG-DPSM is used to model ultrasonic field emission and damage detection in case of isotropic plates produced by finite dimension transducers. The conventional DPSM method uses displacement Green's function solution for each set of source and target points to calculate stress and displacement fields near fluid-solid interface. Note that the DPSM is not a data-driven technique rather it is physics-based technique that uses point sources to generate the fields. The main constituent of DPSM is Green's function solution which is a highly nonlinear function. Despite the fact that, the DL has been around for decades but recently PINNs have become a prominent method to solve physics-based problems. The PINN leverages the automatic differentiation capabilities to differentiate NN with the input coordinates and model parameters. Generally, it uses the governing physics-based equation to train the network which in turn solves nonlinear PDEs. The motivation of the current research work arises from the applicability of PINN in solving complex nonlinear equations efficiently. In the present work, PINN is used to train the NN and further, it utilizes the automatic differentiation to compute the derivate of Green's function solutions. Essentially, the Green's function solution is computed and further the derivative of Green's function with respect to each coordinate axis is performed to find the stress fields. Although, Green's function is symmetrical for each of the P-wave and S-wave, calculation of the derivative function is still a comparatively rigorous task

to do. Simultaneously, for each set of source and target points, the derivative is calculated with respect to each x_1, x_2, x_3 direction [14]. For a group of source and target points, source strength is calculated using the matrix inversion technique. NG-DPSM uses the governing physics of displacement Green's function to train the DL model to evaluate the ultrasonic fields. Initially, the deep NN is trained to predict displacement Green's function solutions separately for both real and imaginary parts for each of the P-wave and S-wave using backpropagation. The learnable parameters (i.e., weights and biases) of the network are trained by embedding the underlying displacement Green's function for each set of source and target points within the loss function. Once, deep NN is trained, the derivatives of Green's function with respect to the coordinates (x_1, x_2 and x_3) are estimated using automatic differentiation. The computed derivative Green's function is then subsequently employed to calculate stress field for different sets of collocation points. Building on the above prepositions, in this work NG-DPSM framework is proposed to model ultrasonic fields and wave propagation in case of healthy and defective isotropic solids near a fluid-solid interface. The advantages of the NG-DPSM over the conventional DPSM can be summarised as follows:

- NG-DPSM uses a DL approach and once the network is trained using the governing physics of Green's function solutions, one can predict the displacement Green's function for any set of coordinates within the domain of the problem geometry.
- It reduces the meticulous task of finding the derivative of displacement Green's function, making the DPSM modelling computationally more efficient. The gradient function of displacement Green's function solutions is computed using DL package such as automatic differentiation.
- The proposed framework is capable of computing ultrasonic fields in both healthy material and in case of a flaw inside solid half-space near fluid-solid interface.
- NG-DPSM is validated for ultrasonic field modelling for different angles of inclination of the transducer surface and different orientations of the circular cavity within the solid. It makes the proposed approach robust for handling various configurations of problem geometry near fluid-solid interface.

2. Background

2.1 Theory of DPSM

The displacement Green's function for isotropic homogeneous solids can be written as [36],

$$G_{ij}(\mathbf{x};\mathbf{y}) = \frac{1}{4\pi\rho\omega^2}\left[\frac{\mathrm{e}^{ik_p r}}{r}\left(\left(k_p^2 R_i R_j + (3R_i R_j - \delta_{ij})\right)\left(\frac{\mathrm{i}k_p}{r} - \frac{1}{r^2}\right)\right)\right.$$
$$\left. + \frac{\mathrm{e}^{ik_s r}}{r}\left(\left(k_s^2(\delta_{ij} - R_i R_j) + (3R_i R_j - \delta_{ij})\right)\left(\frac{\mathrm{i}k_s}{r} - \frac{1}{r^2}\right)\right)\right], \tag{1}$$

where, $R_i = (x_i - y_i)/r$; x_i and y_i are the coordinates of the observation point and source point respectively, $r = |\mathbf{x} - \mathbf{y}|$ is the magnitude of distance between observation and source point, k_p and k_s refer to the P- and S-wave numbers of the solid, respectively.

When a point source excitation acts in $\mathbf{y}$ direction then the displacement field at $\mathbf{x}$ can be expressed using space dependent Green's function $G_{ij}(\mathbf{x};\mathbf{y})$ as,

$$u_i = U_i \mathrm{e}^{-i\omega t} = G_{ij}(\mathbf{x};\mathbf{y}) P_j \mathrm{e}^{-i\omega t}. \tag{2}$$

The stress Green's function at $\mathbf{x}$ in a homogeneous solid due to a concentrated time dependent harmonic force at $\mathbf{y}$ can be expressed as,

$$\sigma_{ij}(\mathbf{x};\mathbf{y}) = \left(\mu(G_{ik,j} + G_{jk,i})\delta_{kq} + \lambda\delta_{ij}G_{kq,k}\right)P_q, \tag{3}$$

where, μ and λ are the two Lame's constants. The stress functions for different sets of i and j values are computed by taking the directional derivative of displacement Green's function and substituting the derivatives in Eq. (3). A comprehensive explanation to the theory of DPSM is found in the Refs[5, 14, 37, 38] and can be helpful to the readers. In the current context, PINN is trained with the physics-based equation given in Eq. (1) to yield a DL model that can estimate Green's function solution. Further, the automatic differentiation is utilised to differentiate the Green's function with respect to the coordinate in order to evaluate stress fields as given in Eq. (3). The mathematical background of PINN is discussed briefly in the following section.

2.2 Design of PINN

In the following section, the mathematical background and the architecture of ANN and PINN are discussed in detail. An ANN is a composition of parameterised nonlinear functions characterised using different number of nodes per layer. According to the *universal function*

approximation theorem [39], NNs can approximate any arbitrary Borel measurable functions. Numerous ways of ANN formulation can be carried out for different sets of problems as discussed in Refs[40-42]. In this paper, a fully connected deep NN is employed that consists of an input layer, several hidden layers, and an output layer. Mathematical representation of a NN in the form of a tensor can be shown as follows:

$$h_{\eta}^{(l)} = \phi_{l-1}\left(\sum_{\xi=1}^{ml-1}\left(w_{\eta,\xi}^{l}\left(h_{\xi}^{l-1}\right)+b_{\eta}^{l}\right)\right), \tag{4}$$

where, h_{η}^{0} and h_{η}^{l} are inputs and outputs of the NN and, $w_{\eta,\xi}^{l}$ and b_{η}^{l} are the weights and biases of each layer. In Eq. (4), ϕ_{l-1} is a nonlinear activation function which is applied layer wise. Since, the NN is used to trace highly non-linear functions, activation function is integrated in every layer to induce nonlinearity throughout the network. Most popular activation functions include rectified linear unit (ReLU), sigmoid, hyperbolic tangent, and Leaky ReLU. The deep NN for the present problem uses hyperbolic tangent activation function defined as,

$$\phi_{l-1} = \tanh(x) = \frac{e^{x}-e^{-x}}{e^{x}+e^{-x}}. \tag{5}$$

Except for the last hidden layer, the linear activation function is adapted. The weight vector $(\mathbf{w})$, the bias vector $(\mathbf{b})$, and the hyperparameter (β) can be collected within a single parameter $\mathbf{q}$ such that:

$$\mathbf{q} = \{\mathbf{w}, \mathbf{b}, \beta\}. \tag{6}$$

All trainable parameters are tuned by minimising the cost function and using the optimisation algorithm. Since, ANN fully relies on data-driven modelling, a large number of datasets is required to train the NN, increasing the meticulous task of data curing and excessive consumption of computational resources. However, PINNs on the other hand uses physical equations and a few numbers of collocation points to train the NN. They have the ability to compile both data-driven modelling and be consistent with the existing physics of the problem. The design of PINN is based on a fully connected deep NN and the governing physics is embedded in the cost function.

The overarching goal of this work is to develop physics-informed learning machines. Toward this goal, we will first delineate the various ways of embedding underlying physics in an ML architecture. Currently, there are three fundamental biases that can be employed individually or in tandem to expedite training and enhance the generalization of ML:

observational, inductive, and learning biases [43]. To begin with, observational biases can manifest the underlying nature of systems using augmented data to learn the vector fields and functions that imitate the physical significance of the data. Further, inductive biases incorporate a prior set of information into the ML architecture to inherently satisfy the physical laws and constraints, but are limited to certain symmetry groups and suffer from the complexity in scaling the model. Finally, learning biases lead to the suitable choice of loss function comprising physics loss and constrains which eventually satisfy the underlying physics that can be expressed in the form of differential, integral, and even fractional equations. In the present work, PINN is used to predict the displacement Green's function solutions and also to calculate the stress fields. It is worth mentioning that Green's function for isotropic solids is nonlinear with respect to the displacement between source and target points. The deep and non-linear architecture of PINN has poised itself as a suitable method to evaluate Green's function solutions. The Green's function solution acts as the governing physics and guides the network while training. The domain of the problem is populated with a large number of point sources and target points. Each set of Green's function solutions are evaluated at target points using PINN. The coordinates (x_i, y_i) are provided as the input of the DL model that predicts the displacement field ($\mathbf{u}$) as the output. The displacement Green's function solutions can be approximated using a nonlinear operator, $\mathrm{N}[\square]$. The mathematical representation of the network can be given as,

$$\mathrm{N}(\mathbf{u}, \beta) = g, \tag{7}$$

where, g is a forcing term. The parameter $\mathbf{q}$ given in Eq.(6) can be obtained by solving an optimisation problem using a set of collocation points (x_i, y_i) defined as,

$$\mathbf{q}^* = \arg\min_{\mathbf{q}} \mathrm{L}(\mathbf{u}; \mathbf{q}), \tag{8}$$

where $\mathrm{L}(\mathbf{u}; \mathbf{q})$ is the mean square loss function (MSL) defined as,

$$\mathrm{L}(\mathbf{u}; \mathbf{q}) = \|\mathrm{L}\|_2^2 = \frac{1}{N}\sum_{k=1}^{N}(\mathrm{N}(\mathbf{u}, \beta) - g)^2. \tag{9}$$

The weight vector $(\mathbf{w})$ and the bias vector $(\mathbf{b})$ are trained by optimising the loss function $\mathrm{L}(\mathbf{u}; \mathbf{q})$ using the backpropagation algorithm. Recently, optimiser such as Adam is widely used as the iterative scheme for the optimisation of loss functions. The gradient of the loss function with respect to each parameter is carried out by automatic differentiation. The workflow of PINN using Green's function solutions as the governing physics is illustrated in Figure 1.

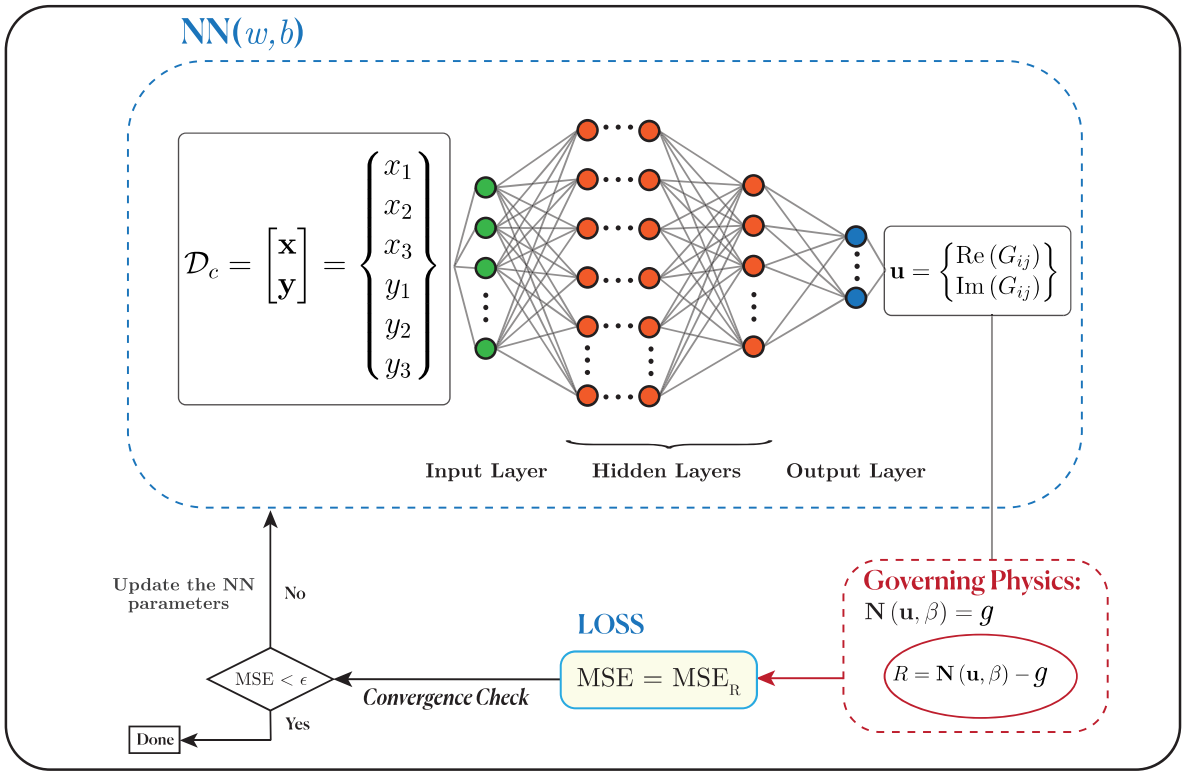

Figure 1. Schematic view of PINN framework using Green's function solutions.

3. Problem Geometry

Let us consider a fluid half-space and a solid half-space with a circular hole separated by a plane interface as shown in Figure 2. The fluid-solid interface can be modelled using two layers of distributed point sources and the hole can be modelled using a single layer of point sources. A circular transducer of finite dimension is placed near the fluid half-space and can be modelled using a single layer of point sources. Total ultrasonic fields inside the solid and the fluid can be calculated using the superposition of fields produced by all these point sources at the target points. The transducer surface is modelled using N number of source points along its surface and M number of target points are distributed along the edge of the interface. Let N_C represents the number of distributed point sources along the periphery of the circular cavity. Each point source that is contributing to the calculation of the ultrasonic field has three different components of force in three different directions. The source strength vectors corresponding to the interface plane, transducer surface and the periphery of the cavity can be calculated using matrix inversion by satisfying all boundary and interface conditions. Considering the problem geometry in Figure 2, $\mathbf{A}_s$ is the source strength vector for point sources distributed just below the transducer surface. $\mathbf{A}_1$ and $\mathbf{A}_1^*$ are the source strength vectors for point sources located just

above and below the interface. The ultrasonic field generated by the cavity is calculated using the source strength vector $\mathbf{A}_c$. For illustration purposes consider two points (L and M) as shown in Figure 2. The ultrasonic field at point L is the summation of the contributions of point sources $\mathbf{A}_s$ and $\mathbf{A}_1$. Likewise, the ultrasonic field at point M is the summation of contributions of point sources $\mathbf{A}_1^*$ and $\mathbf{A}_c$. A global system of equations is formed by satisfying the boundary conditions at the cavity and the transducer surface, and continuity conditions across the fluid-solid interface. The detailed DPSM formulation satisfying the fluid-solid interface conditions, and boundary conditions along the periphery of the cavity and the transducer face is omitted herein for brevity and can be found elsewhere [5, 14, 44]. The stress field matrix along the periphery of the cavity is calculated by using stress transformation laws for the rotated coordinate system briefly discussed in Refs[4, 44]. The source strength vectors $\mathbf{A}_s$, $\mathbf{A}_1$, $\mathbf{A}_1^*$ and $\mathbf{A}_c$ are computed by solving the generated system of equations using the appropriate matrix inversion operation. Then the source strength vectors are employed to calculate the displacement, stress, pressure, and velocity fields at any point within the regime of the problem geometry.

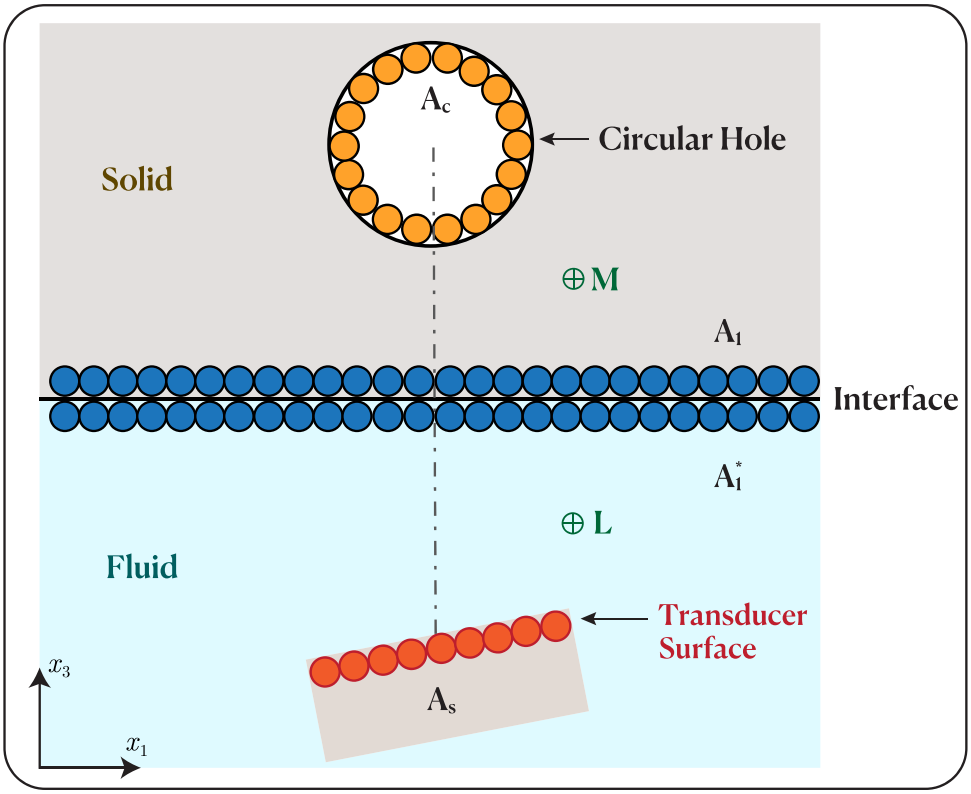

Figure 2. Problem geometry for distributed point source modelling near fluid-solid interface having a circular hole in the solid half-space.

4. Construction of NG-DPSM framework using PINN

The PINN framework allows to invoke certain physical laws and constitutive relations in the NN in the form of the loss function. The physical equations and the boundary conditions are modelled using nonlinear operators. Loss function comprising physics loss and other constrain losses is optimised to predict the output fields. The pioneering work done by Raissi, *et al.* focuses on predicting the solutions of PDEs [27]. PINNs are primarily employed to solve various scientific and engineering problems where the governing equations are in the form of differential equations [29, 45]. The capability of PINN can be further extended to solve problems where the governing physics is in the form of fractional equation. The advantage of PINN in solving fractional equations and nonlinear equations have been well illustrated in the literature [43, 46]. Meng and Karniadakis demonstrated the application of PINN in solving nonlinear equations using multi-fidelity PINN (mfPINN) [46]. Kalimullah, *et al.* utilized the mfPINN to predict AE localization in case of sparse measurements [47]. The proposed NG-DPSM framework uses Green's function solutions as the governing physics to train the model parameters and utilizes the capability of automatic differentiation for calculating the gradient function of displacement fields.

In the DPSM modelling the transducer surface and the solid-fluid structure are modelled by point sources distributed along different planes. If the numbers of source points and target points are n_1 and n_2 respectively, then a total number of $(n_1 n_2)$ Green's function evaluation is required for modelling the ultrasonic field. Each source and target point can be identified using its coordinate values x_1, x_2, x_3 and y_1, y_2, y_3. The coordinates of source and target points are defined using a normalised vector between the two point sources $R_i = (x_i - y_i)/r$ where, r can be expressed as:

$$r = |\mathbf{x} - \mathbf{y}| = \sqrt{(x_1 - y_1)^2 + (x_2 - y_2)^2 + (x_3 - y_3)^2}. \tag{10}$$

The NG-DPSM approach uses a set of collocation points (x_i, y_i) for the existing physics of the DPSM modelling to train the network. The displacement Green's function for solid is the governing physics behind NG-DPSM framework. Initially, the input for the construction of feed-forward NN is given as (x_i, y_i) where $i = 1, 2, 3$. The physics of the problem can be expressed using a non-linear operator $\mathrm{N}[\square]$ as given in Eq. (7). The $\mathbf{u}$ in Eq. (7) is the ouput of the network consisting of real and imaginary values of Green's function solutions as $\mathrm{Re}(G_{ij})$ and $\mathrm{Im}(G_{ij})$, and β is any arbitrary parameter associated with the physics of the

problem. In the present framework, β comprises of density (ρ), frequency (ω) and the wave numbers (k_p and k_s) for P-wave and S-wave, g is a forcing term which is considered as zero. In this case, the nonlinear Green's function, which is used as the governing physics to train the netwrok, is given in Eq.(1). The stress function to be calculated can be approximated using the NN as,

$$\sigma_{ij}(\mathbf{x};\mathbf{y}) \approx \left(\mu \left(\frac{\partial \mathrm{N}(\mathbf{u},\beta)}{\partial x_j} + \frac{\partial \mathrm{N}(\mathbf{u},\beta)}{\partial x_i} \right) \delta_{kq} + \lambda \delta_{ij} \frac{\partial \mathrm{N}(\mathbf{u},\beta)}{\partial x_k} \right) P_q. \tag{11}$$

The network hyperparameters are updated by computing a residual. The residual for this case is given as,

$$\mathsf{R} = \mathrm{N}(\mathbf{u},\beta) - g. \tag{12}$$

While evaluating the ultrasonic fields using NG-DPSM, for the optimal performance of the network, MSL function is taken as the cost function to train the NN parameters. The MSL function for NG-DPSM can be defined as,

$$\mathrm{MSL} = \|\mathsf{R}\|_2^2 = \frac{1}{N} \sum_{k=1}^{N} (\mathrm{N}(\mathbf{u},\beta))^2, \tag{13}$$

here, N represents the number of collocation points for which the Green's function solution is predicted. The physics loss function L_p is defined as the summation of real and imaginary loss functions as,

$$\mathrm{L}_p = \mathrm{L}_{\mathrm{Re}} + \mathrm{L}_{\mathrm{Im}}, \tag{14}$$

where, L_{Re} and L_{Im} represent the loss functions corresponding to the real and imaginary parts of displacement Green's function, respectively for both P-wave and S-wave and can be expressed as,

$$\mathrm{L}_{\mathrm{Re}} = \frac{1}{N} \sum_{k=1}^{N} \left\| \mathrm{Re}(G_{ij}) \right\|_2^2, \tag{15}$$

$$\mathrm{L}_{\mathrm{Im}} = \frac{1}{N} \sum_{k=1}^{N} \left\| \mathrm{Im}(G_{ij}) \right\|_2^2, \tag{16}$$

where, $\mathrm{Re}(G_{ij})$ and $\mathrm{Im}(G_{ij})$ can be obtained by decomposing the harmonic term associated with the displacement Green's function solutions using the Euler's identity. The total displacement Green's function can be written as the summation of P-wave and S-wave as,

$$G_{ij}(\mathbf{x};\mathbf{y}) = Gp_{ij}(\mathbf{x};\mathbf{y}) + Gs_{ij}(\mathbf{x};\mathbf{y}). \tag{17}$$

Now, decomposing the harmonic terms for both P-wave and S-wave using Euler's identity gives,

$$\left.\begin{aligned} \mathrm{e}^{\mathrm{i}k_p r} &= \cos(k_p r) + \mathrm{i}\sin(k_p r) \\ \mathrm{e}^{\mathrm{i}k_s r} &= \cos(k_s r) + \mathrm{i}\sin(k_s r) \end{aligned}\right\}. \tag{18}$$

Substituting Eq. (18) in Eq. (1) and rearranging the real and imaginary parts of Green's function for both P-wave and S-wave, $\mathrm{Re}(G_{ij})$ and $\mathrm{Im}(G_{ij})$ can be expressed as,

$$\begin{aligned} \mathrm{Re}(G_{ij}) = &\left[\left(\frac{k_p^2 R_i R_j}{r} - \frac{(3R_i R_j - \delta_{ij})}{r^3}\right)\cos(k_p r) - \left(\frac{k_p(3R_i R_j - \delta_{ij})}{r^2}\right)\sin(k_p r)\right] + \\ &\left[\left(\frac{k_s^2 R_i R_j}{r} + \frac{(3R_i R_j - \delta_{ij})}{r^3}\right)\cos(k_s r) + \left(\frac{k_s(3R_i R_j - \delta_{ij})}{r^2}\right)\sin(k_s r)\right], \end{aligned} \tag{19}$$

$$\begin{aligned} \mathrm{Im}(G_{ij}) = &\left[\left(\frac{k_p(3R_i R_j - \delta_{ij})}{r^2}\right)\cos(k_p r) + \left(\frac{k_p^2 R_i R_j}{r} - \frac{(3R_i R_j - \delta_{ij})}{r^3}\right)\sin(k_p r)\right] + \\ &\left[\left(\frac{k_s(\delta_{ij} - 3R_i R_j)}{r^2}\right)\cos(k_s r) + \left(\frac{k_s^2 R_i R_j}{r} + \frac{(3R_i R_j - \delta_{ij})}{r^3}\right)\sin(k_s r)\right]. \end{aligned} \tag{20}$$

The total physics loss is then given as,

$$\mathrm{L}_p = \frac{1}{N}\sum_{k=1}^{N}\left[\left\|\mathrm{Re}(G_{ij})\right\|_2^2 + \left\|\mathrm{Im}(G_{ij})\right\|_2^2\right]. \tag{21}$$

To ensure the vanishing shear stress properties near the fluid-solid interface, additional boundary loss is considered as,

$$\mathrm{L}_{bc} = \frac{1}{N}\sum_{k=1}^{N}\left[\mu\left(\left\{\left\|\mathrm{Re}(G_{ij,k})\right\|_2^2 + \left\|\mathrm{Im}(G_{ij,k})\right\|_2^2\right\} + \left\{\left\|\mathrm{Re}(G_{ij,i})\right\|_2^2 + \left\|\mathrm{Im}(G_{ij,i})\right\|_2^2\right\}\right)\right]. \tag{22}$$

Therefore, the total loss function is the summation of physics loss and the boundary condition loss,

$$\mathrm{L}_{total} = \mathrm{L}_p + \mathrm{L}_{bc}. \tag{23}$$

The loss function is minimised using the optimisation algorithm to predict displacement fields. In each epoch certain number of coordinates are trained using minibatches of datasets, making the hyperparameters (weights and biases) to train efficiently using the governing physics. Once the network is trained, the real and imaginary values of displacement Green's function solution can be predicted for different sets of (x_i , y_i). The predicted Green's function solution gives the total displacement fields using DPSM modelling. For calculating stress

fields, the present NG-DPSM framework leverages the capability of NN to predict its derivative function since, the computation of stress field is done by taking the directional derivative of the displacement Green's function. Therefore, the derivative of displacement Green's function solutions needed to be evaluated for each set of source and target points. The conventional DPSM uses rigorous differentiation of displacement Green's function with respect to different *x*-coordinates. After computing displacement field, the proposed framework calculates the gradient function of Green's function solutions corresponding to x_1, x_2 and x_3 using automatic differentiation expressed as,

$$\nabla \mathbf{u} = \begin{Bmatrix} \mathrm{Re}(G_{ij,k}) \\ \mathrm{Im}(G_{ij,k}) \end{Bmatrix}, \tag{24}$$

$$G_{ij,k} = \mathrm{Re}(G_{ij,k}) + \mathrm{Im}(G_{ij,k}). \tag{25}$$

The computed gradient fields are then substituted in Eq.(3) to predict the stress fields. The estimated displacement Green's functions and the stress fields for each set of distributed points are utilized to predict total ultrasonic fields within the problem geometry using DPSM. The schematic view of proposed NG-DPSM approach to predict Green's function solutions, stress fields and total ultrasonic fields is shown in Figure 3. Note that, in NG-DPSM the PINN is trained by informing displacement Green's function within the domain of problem geometry. Once the PINN is trained, it can be employed to solve range of problems with different forcing functions and boundary conditions within the training domain.

The NN is efficient in modelling Green's function solutions but the tuning of hyperparameters such as number of hidden layers, nuerons per layer, learning rate, etc. is done iteratively. It should be noted that several other methods such as random search and Bayesian hyperparameter optimisation [48] are available to tune the hyperparameters. Despite, these probablistic approach, the NN might not be able to learn the optimal value of parameters to achieve the desired accuracy. The number of hidden layers along with the number of neurons per hidden layer is progressively increased to an upper threshold (20 in the numerical examples). Additional hidden layers can be introduced in the network until no further decrement in the MSL value is observed.

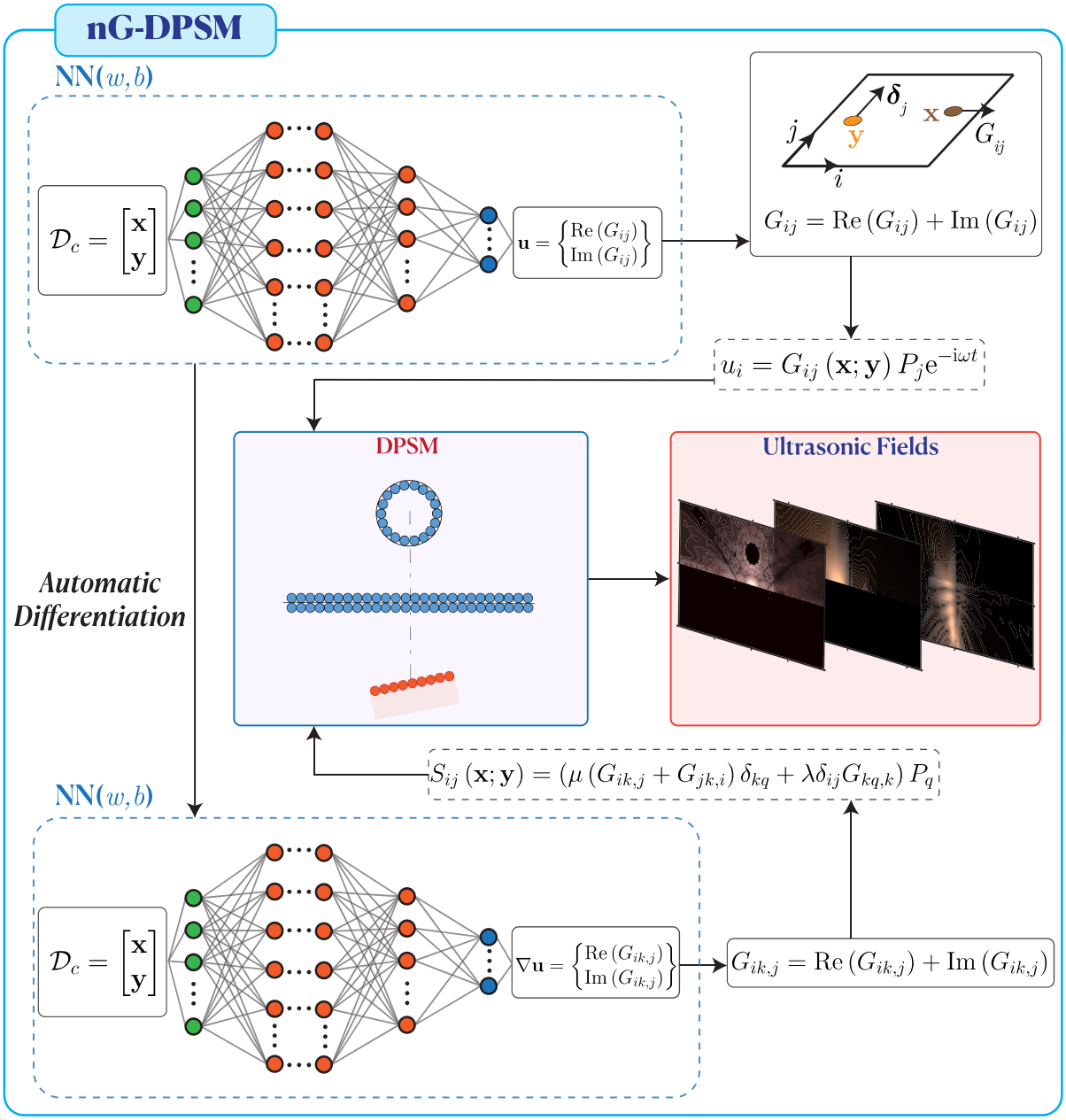

Figure 3. The schematic view of proposed NG-DPSM framework

5. Results and Discussion

In this section, to illustrate the applicability and efficacy of the proposed framework for different complex scenarios such as various locations of defect, frequencies, and numerous transducer angles. The ultrasonic fields near fluid-solid interface of an isotropic plate are presented in Sections 5.1 and 5.2. In section 5.1, the pressure and stress fields near the fluid-solid interface is calculated for numerous transducer angles. Further, the Section 5.2 presents the ultrasonic fields, evaluated for different locations of the circular cavity and for different

frequencies using the proposed method. The accuracy and efficiency in producing the ultrasonic fields by NG-DPSM and by the conventional DPSM are discussed for both cases.

5.1 Ultrasonic fields near fluid-solid interface having no defect

A numerical study is conducted where the problem geometry consists of an aluminium half-space over a water half-space. The density and speed of the wave in water are 1 g/cc and 1.48 km/s, respectively. The density of aluminium is taken as 2.7 g/cc and, the P-wave and S-wave velocities are 6.5 km/s and 3.13 km/s, respectively. The length of the fluid-solid interface in $x-$direction is taken as 50 mm. The dimension of each of both the solid and fluid media in the $z-$direction is taken as 4 mm. Ultrasonic fields are generated by the transducer of finite dimension having a diameter of 4 mm placed inside the fluid half-space at various angles of inclination with respect to the fluid-solid interface. The width of the fluid-solid interface in the $y-$direction or out-of-plane direction is considerably larger than the diameter of the transducer. It is to be noted that this three-dimensional problem is solved by the proposed framework and ultrasonic fields are plotted along the vertical plane of symmetry (xz plane) of the problem geometry. The problem geometry and the distributed point sources are shown in Figure 2. Ninety-five point sources are placed on each side of the interface. Three lines of such point sources are considered in the $y-$direction or the out-of-plane direction of Figure 2. One hundred point sources are distributed behind the transducer surface.

The Green's function solution for the source points is calculated within the DPSM framework. Conventionally, significant computational time is required to compute the Green's function solution for the aforementioned points. The distance between the point sources, the maximum spacing allowed between neighbouring points and the minimum number of point sources required for the convergence criteria of the DPSM solution have been studied in Refs [49-52]. The convergence criterion suggests that the distance between two neighbouring points should be less than the wavelength in the fluid divided by $\sqrt{\pi}$ as given in Ref [38]. In the present problem geometry, the point sources are distributed such that the distance (Δ) between the two neighbouring points is less than $\left(\lambda/2\sqrt{\pi}\right)$.

To simplify this computational intricacy, we employed a DL architecture based on PINN to compute the displacement Green's function and stress fields. In the present study, the network architecture consisting of six inputs and nine hidden layers with 20 neurons each is considered. The six inputs of the network are the coordinates of distributed points

corresponding to each source and target planes. The output of the network is G_{ij}. Hyperbolic tangent (tanh) activation function is used for each layer except for the last layer, the linear activation function is utilised. Loss function is minimised using the governing physics of the displacement Green's function. The NN is trained using collocation points as different sets of source and target points. The loss function is optimised using Adam optimiser, having a learning rate and decay rate of 0.01 and 0.005, respectively. The network is trained for sets of data points for the prediction of $G_{11}, G_{12}, G_{13}, G_{22}, G_{23}$ and, G_{33}. The performance of the optimization algorithm while training the network for 3000 epochs is shown in Figure 4. It can be observed from Figure 4, the loss function converges rapidly as the number of epochs increases. The value of MSL function as defined in Eq. (23) after 3000 epochs is 2.7677e^{-05}.

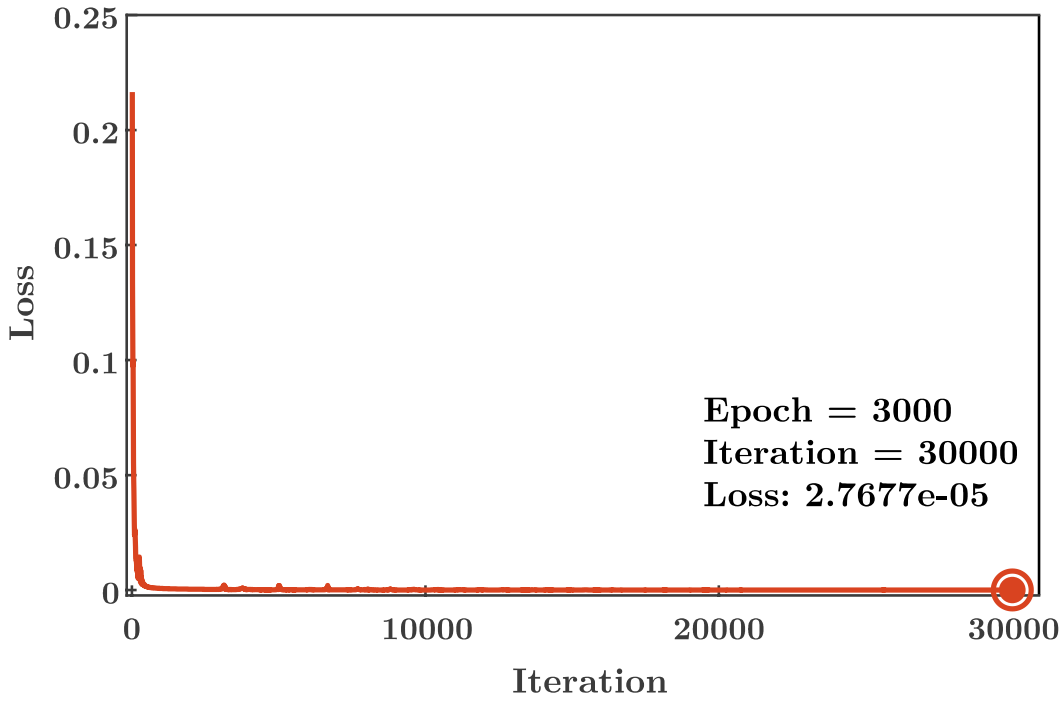

Figure 4. The performance summary of the optimization algorithm during the training of the DL architecture.

The displacement Green's function solutions can be predicted after successful training of the NN. The predicted values of Green's function, G_{ij} are calculated using the PINN. Figure 5 shows the displacement Green's function (i.e., $G_{11}, G_{12}, G_{13}, G_{22}, G_{23}$ and G_{33}) using the closed form Green's function solution as the true solution and predicted values as PINN solutions. The difference between the true and predicted PINN solutions are observed to be in the order

of magnitude of 10^{-3} to 10^{-4} which can generally be ignored. It can be observed that the true solutions and the PINN results are in good aggrement with each other.

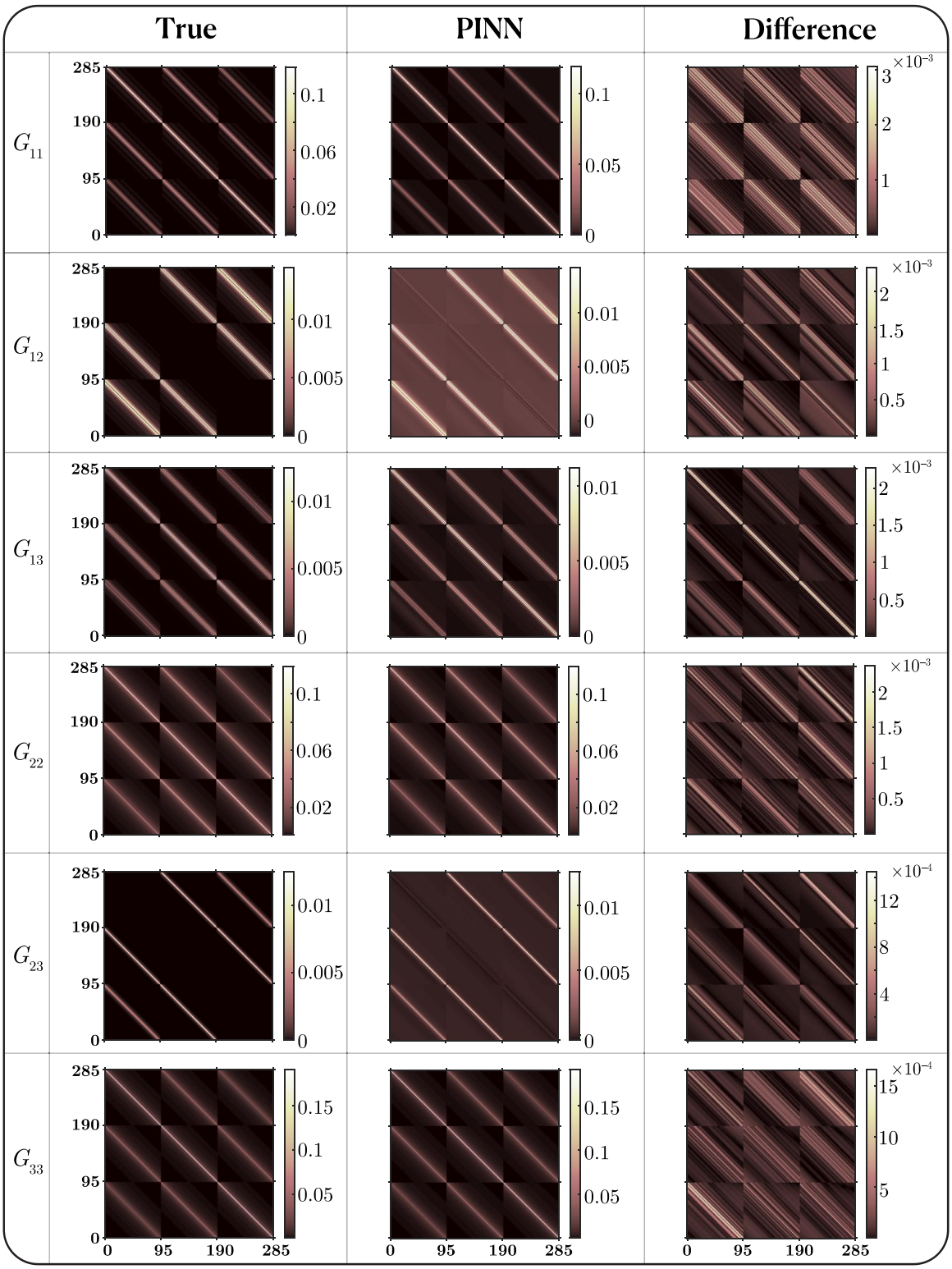

Figure 5. The displacement Green's function solution for isotropic solids using (a) analytical displacement Green's function solutions, (b) PINN, and (c) relative error.

The trained deep NN is incorporated within the DPSM to yield proposed NG-DPSM framework. The DL architecture of NG-DPSM framework primarily provides two advantages. The calculation of displacement Green's function solutions took 0.05 second in MATLAB® R2022b in an 8 core Apple M1 processor with 16GB RAM after training. On the contrary, the conventional method took 3 seconds to evaluate Green's function solutions performed on the same machine configuration. It is worth noting that the computational intricacy in computing the Green's function solutions using the PINN method is thus reduced significantly by sixty times.

Finally perhaps most importantly, the automatic differention capability of NN substitutes the computational intensive analytical evaluation of gradients in conventional DPSM to predict the pressure and stress fields. The gradient of the output of the network, i.e., G_{ij} is calculated with respect to each coordinate axis, $\mathbf{x} = \{x_1, x_2, x_3\}^T$. These DL evaluated derivative of Green's function solutions are substituted in Eq. (3) to compute the stress field at $\mathbf{x}$ for the concentrated harmonic force applied at $\mathbf{y}$. Once ultrasonic fields for each set of source and target points are evaluated, the total ultrasonic fields generated by the transducer surface in presence of the fluid-solid interface can be calculated using the source strength matrix.

The ultrasonic fields are predicted for transducer frequency $(f = 1\text{MHz})$ for different angles of inclination of the transducer surface with respect to the fluid-solid interface using the proposed NG-DPSM framework. The scattered fields for the critical angle $(\Theta_{cr} = 30.42^\circ)$ for the water-aluminum interface, less than the critical angle $(\Theta < \Theta_{cr})$ and greater than the critical angle $(\Theta > \Theta_{cr})$ of inclination of transducer surface are computed using both conventional DPSM and NG-DPSM approach. The normal stresses are shown as the normalised amplitude with respect to the source strength. The normalised difference between the two solutions is obtained with respect to the infinity norm of the DPSM solutions as shown below,

$$Difference = \frac{[(\text{DPSM}) - (\text{nG-DPSM})]}{\|\text{DPSM}\|_\infty}. \tag{26}$$

Top two rows of Figure 6 show the normal stresses (**s11**, **s33**) in aluminium and the pressure field in water while the bottom row shows the vertical displacement (**u3**) for an angle of inclination less than the critical angle $(\Theta = 15.24^\circ < \Theta_{cr})$.

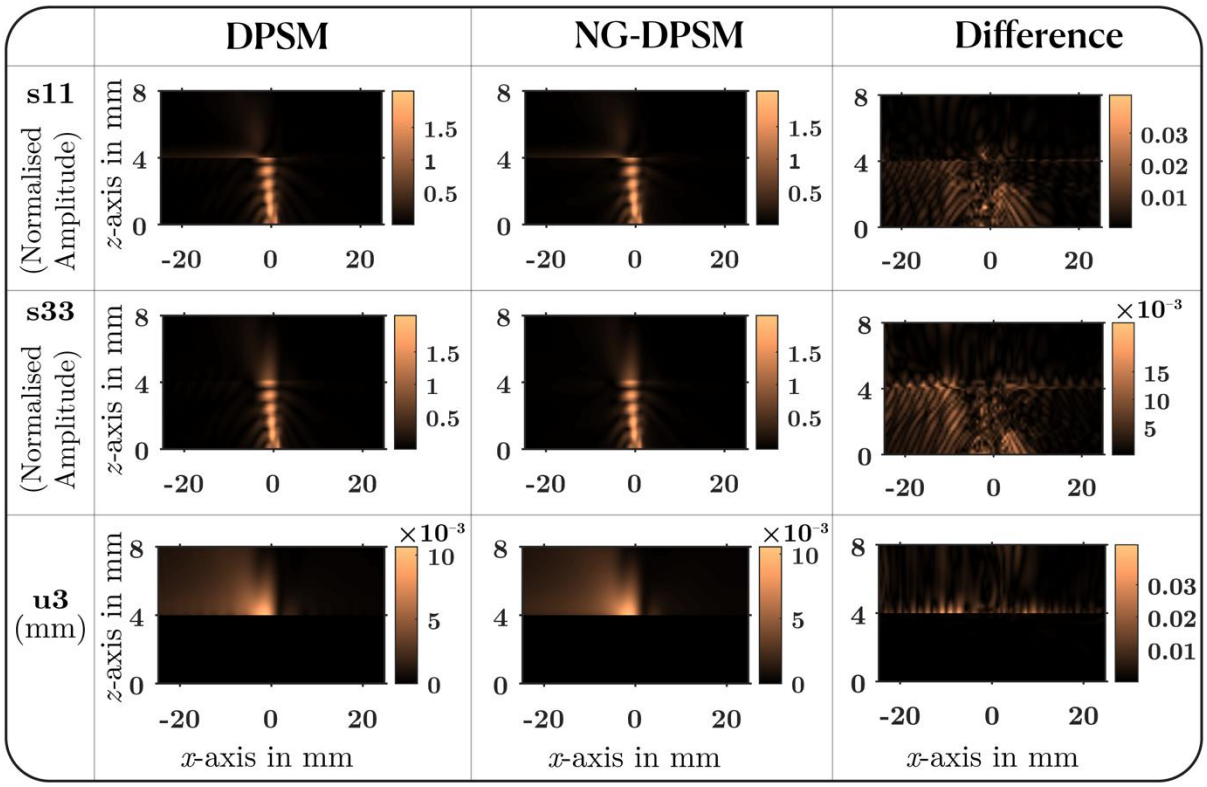

Figure 6. Top two rows show normal stresses $(\mathbf{s11}, \mathbf{s33})$ and the bottom row shows the displacement field $(\mathbf{u3})$, computed using the conventional DPSM (column 1), NG-DPSM (column 2), and normalised difference (column 3) for 1 MHz transducer frequency for angle of inclination, $(\Theta < \Theta_{cr})$.

It can be seen in Figure 6 that the results obtained by NG-DPSM are in close agreement with the conventional DPSM results. The difference between these two solutions is less than 1% ($\sim 10^{-3}$) along the line of collimation of waves for both stress and displacement fields. Comparatively, the difference is more for the far field waves which can be improved further at the cost of computational efficacy obtained by the proposed method. It is known that the penetration depth of the guided wave is proportional to the wavelength; in other words, if the frequency of the signal decreases its wavelength increases, and in turn the penetration depth of the guided wave increases. Figure 7 and Figure 8 show the ultrasonic fields for two other angles of inclination - critical angle $(\Theta = \Theta_{cr})$ and greater than critical angle $(\Theta > \Theta_{cr})$. Similar inferences can be drawn about the accuracy of these two cases. For the angle of inclination equal to or greater than the critical angle, one can notice that more energy is either propagated along the interface as leaky Rayleigh wave (Figure 7) or reflected back to the water half-space (Figure 8) compared to the subcritical angle of incidence case (Figure 6).

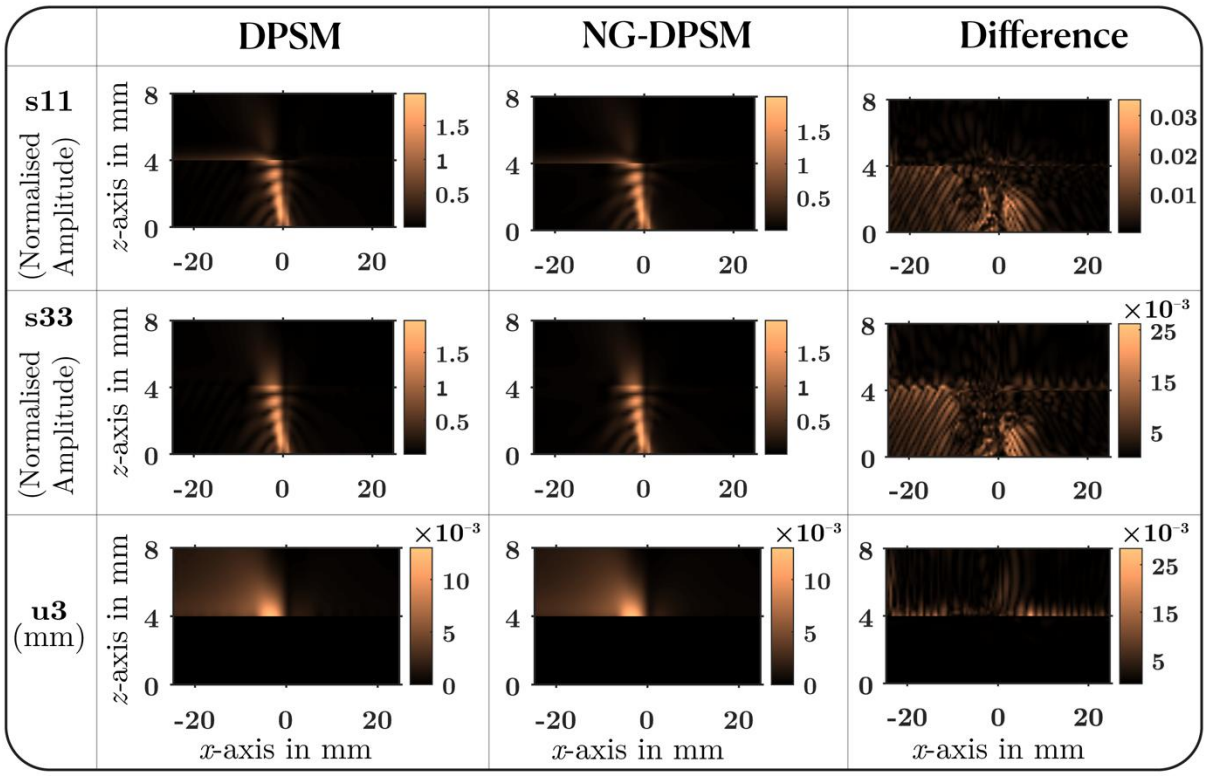

Figure 7. Top two rows show normal stresses $(\mathbf{s11},\mathbf{s33})$ and the bottom row shows the displacement field $(\mathbf{u3})$, computed using the conventional DPSM (column 1), NG-DPSM (column 2), and normalised difference (column 3) for 1 MHz transducer frequency for angle of inclination, $(\Theta = \Theta_{cr})$.

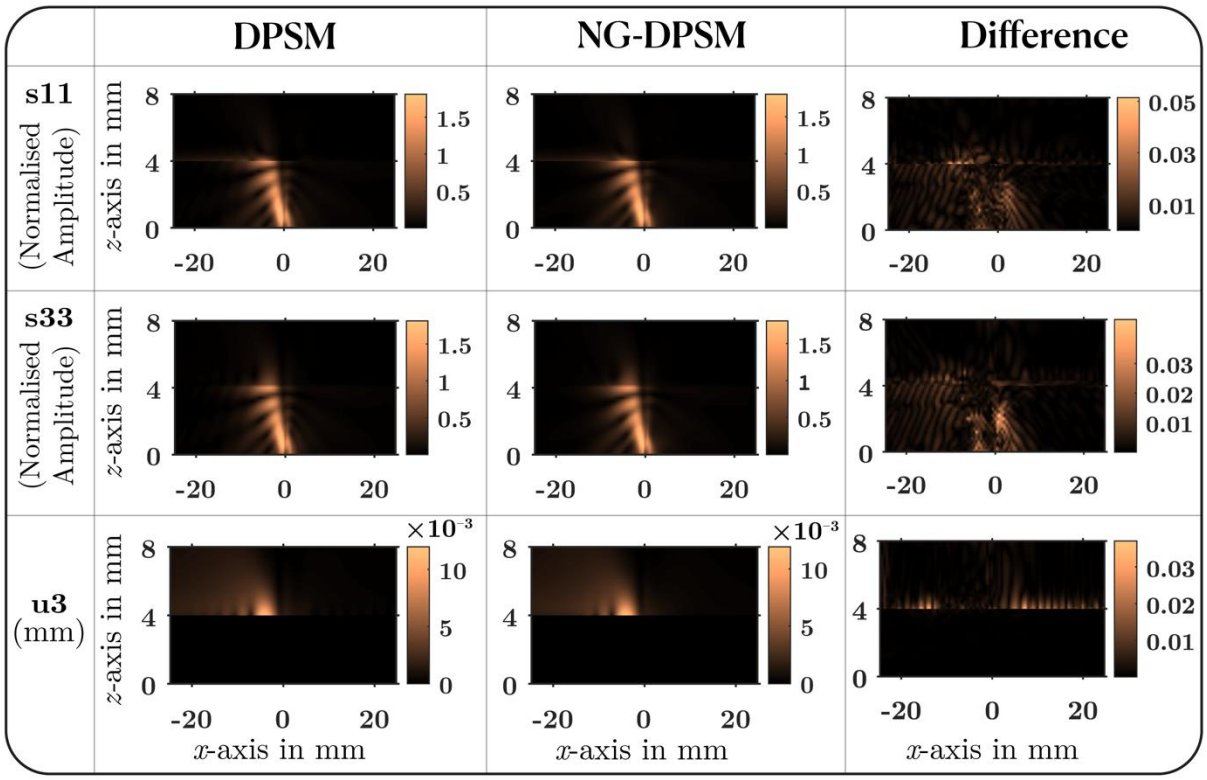

Figure 8. Top two rows show normal stresses $(\mathbf{s11}, \mathbf{s33})$ and the bottom row shows the displacement field $(\mathbf{u3})$, computed using the conventional DPSM (column 1), NG-DPSM (column 2), and normalised difference (column 3) for 1 MHz transducer frequency for angle of inclination, $(\Theta > \Theta_{cr})$.

5.2 Distribution of ultrasonic fields in presence of a circular hole in the solid half-space.

Next, the numerical study is carried for a homogeneous isotropic half-space having a circular shaped cavity in the solid half-space. The problem geometry and the materials are same as the defect-free case discussed in Section 0. Length of the interface in this case is taken as 40 mm in $x-$direction and the thicknesses of both the solid and the fluid layers in the $z-$direction is taken as 10 mm. The objective of this study is to investigate the scattered ultrasonic fields generated by the defect using the NG-DPSM approach. The ultrasonic fields are produced using finite size transducer of 4 mm diameter. The transducer surface is discretised using 110-point sources. At the fluid-solid interface, 125-point sources are distributed on each side of the interface plane. The circular hole can be modelled by placing n number of point sources along the periphery of the cavity. The value of n depends on the size of the hole. To ensure the convergence criteria (i.e., spacing between two adjacent point sources $<$ ($\frac{1}{3}$)rd of wavelength) the number of point sources increase with the cavity size. The scattered fields for

different locations of the circular hole are modelled for transducer frequencies of 1MHz and 2.25MHz. Ultrasonic fields are computed along the plane of symmetry of the problem geometry. Results plotted are along the $z-x$ plane of the problem geometry.

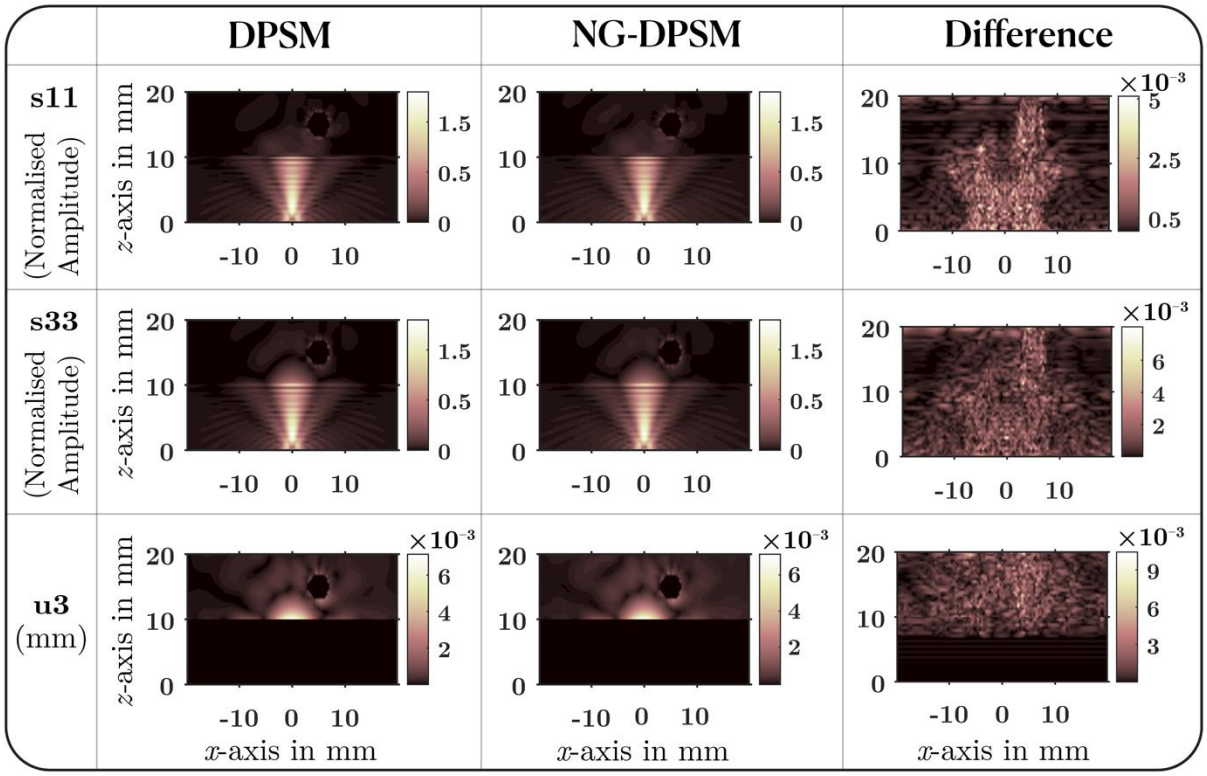

Figure 9. Top two rows show normal stresses $(\mathbf{s11},\mathbf{s33})$ and the bottom row shows the displacement field $(\mathbf{u3})$, computed using the conventional DPSM (column 1), NG-DPSM (column 2), and normalised difference (column 3) for 1 MHz transducer frequency.

The displacement Green's function solution is predicted using the proposed NG-DPSM to calculate ultrasonic fields. Similar steps as delineated in the previous case are followed to obtain various ultrasonic fields, the only change here is the architecture of the NN. Here, the network consists of 12 layers having 20 neurons per layer. For each layer hyperbolic tangent (tanh) activation function is used, except for the last layer where linear activation function is applied. The network is trained for each set of source and target points using the governing physics of displacement Green's function. Loss function is optimised using Adam optimiser and learning rate and decay rate is kept same as the previous case. In this case, the value of MSL function reached $3.1556e^{-05}$ after 3000 epochs.

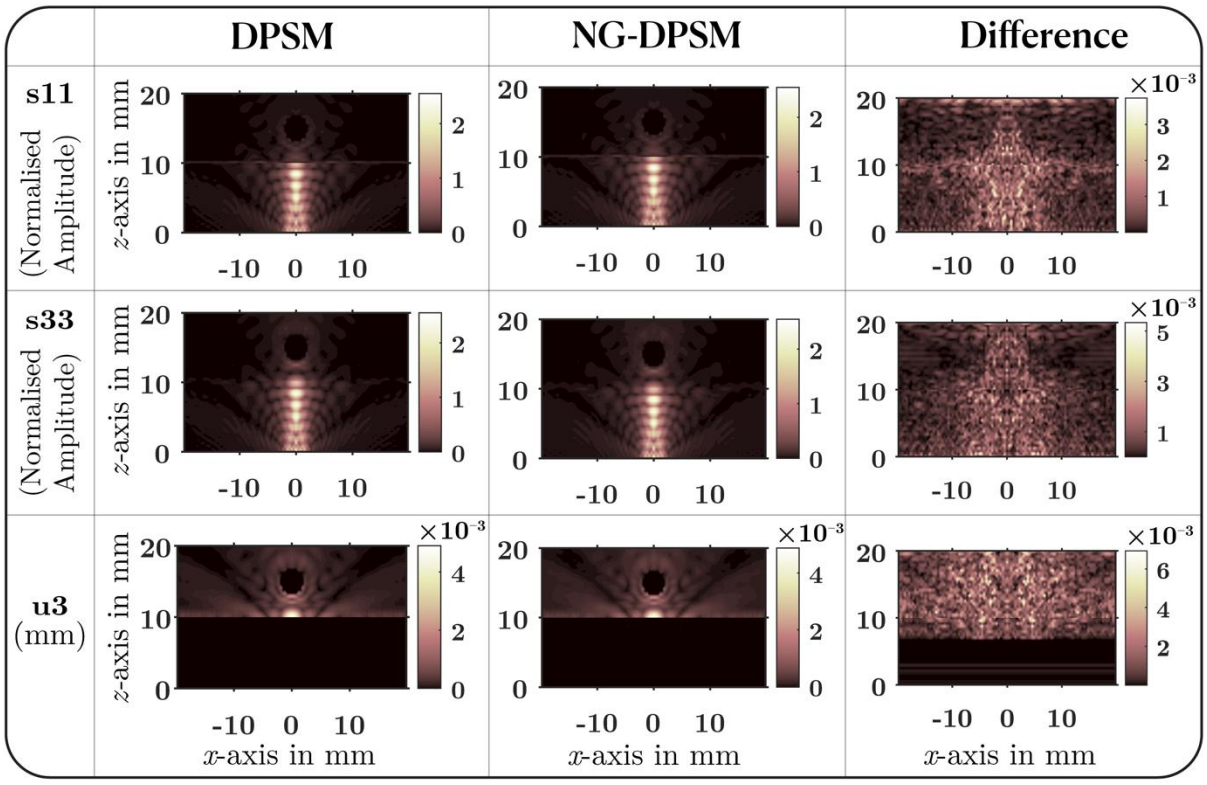

Figure 10. Top two rows show normal stresses $(\mathbf{s11}, \mathbf{s33})$ and the bottom row shows the displacement field $(\mathbf{u3})$, computed using the conventional DPSM (column 1), NG-DPSM (column 2), and normalised difference (column 3) for 2.25 MHz transducer frequency.

Once the network is trained, the gradient function of Green's function solution is evaluated using automatic differentiation. Further, the computed fields are used to predict the source strength vector using the matrix inversion to model total ultrasonic fields using DPSM. Top two rows of Figure 9 show the normal stresses ($\mathbf{s11}$, $\mathbf{s33}$) in aluminium and pressure in water and and the bottom row shows the vertical displacement ($\mathbf{u3}$) for 1 MHz transducer frequency plotted in the $z-x$ plane. The position of the center of the hole is at $x=5$ mm and $z=15$ mm. Scattered ultrasonic fields are clearly visible near the fluid-solid interface and around the periphery of the circular hole. The normalised difference between the true and the predicted solutions is less than 1% (in the order of 10^{-3}). It can be seen that the plots of ultrasonic fields for both DPSM and proposed NG-DPSM framework match satisfactorily. Figure 10 shows similar plots for the transducer frequency of 2.25 MHz. The position of the center of the hole in this case is changed to $x=0$ mm and $z=15\text{mm}$. The ultrasonic fields are scattered symmetrically as the orientation of the hole and the excitation field make the problem symmetrical about the z-axis. Results obtained using both conventional DPSM and NG-DPSM

are compared and the normalised difference is again found to be less than 1%. Hence, from all these examples it can be concluded that NG-DPSM method is capable of replacing the DPSM technique.

6. Conclusion

In this study, we propose a neural Green distributed point source method (NG-DPSM) to simulate ultrasonic fields using a physics informed deep learning approach. Green's function is the main constituent in modelling distributed point source to predict the ultrasonic fields in solids and fluids. Depending on the number of point sources used in the modelling, a large number of Green's function solutions might be needed to be evaluated for different sets of source and target points. A PINN is constructed for the prediction of displacement Green's function where closed form Green's function solutions act as the governing physics in training the network. The network is initiated with six input variables as coordinate vectors for each source point - target point combination (x_i, y_i). It then produces output as displacement Green's function in real and imaginary planes. Once the network is trained, it can be observed that the computational time for displacement Green's function calculation reduces significantly by sixty times. Further, it allows the flexibility of fine spacing of point sources for interface and transducer surfaces. The stress functions are calculated by leveraging the automatic differentiation capability of NNs, on the contrary the rigorous differentiation of Green's function solutions is needed in conventional DPSM. It is an advantage of the proposed approach over the existing DPSM formulation, in terms of computational cost. Numerical investigations are carried out by simulating ultrasonic fields in homogeneous isotropic solids for the case i.e., (a) having no defect and (b) having a circular hole in the solid half-space to illustrate the efficacy. The ability of NG-DPSM is verified for different transducer frequencies and angles of inclination of the transducer surface. It is worth noting that the ultrasonic fields computed using the proposed approach match satisfactorily with the DPSM results. The scattered wave fields around the periphery of the circular cavity using both the NG-DPSM and the conventional DPSM show good matching confirming its applicability for modelling relatively complex geometries with scatterers. Therefore, it is verified that the proposed NG-DPSM approach is a robust and efficient technique for modelling ultrasonic fields for different problem geometries.

Acknowledgement

Amit Shelke, Nur M M Kalimullah and Ayush Thakur would like to acknowledge Indian Space Research Organisation (ISRO) for supporting this work under Grant Number ISRO/RES/ STC/IITG/2021-22.

Reference:

[1] M.R. Jolly, A. Prabhakar, B. Sturzu, K. Hollstein, R. Singh, S. Thomas, P. Foote, A. Shaw, Review of non-destructive testing (NDT) techniques and their applicability to thick walled composites, Procedia CIRP, 38 (2015) 129-136.

[2] T. Kundu, S. Das, S.A. Martin, K.V. Jata, Locating point of impact in anisotropic fiber reinforced composite plates, Ultrasonics, 48 (2008) 193-201.

[3] S. Banerjee, T. Kundu, D. Placko, Ultrasonic field modeling in multilayered fluid structures using the distributed point source method technique, (2006).

[4] S. Banerjee, T. Kundu, Elastic wave field computation in multilayered nonplanar solid structures: A mesh-free semianalytical approach, The Journal of the Acoustical Society of America, 123 (2008) 1371-1382.

[5] S. Banerjee, T. Kundu, Ultrasonic field modeling in plates immersed in fluid, International Journal of Solids and Structures, 44 (2007) 6013-6029.

[6] S. Banerjee, T. Kundu, Semi-analytical modeling of ultrasonic fields in solids with internal anomalies immersed in a fluid, Wave Motion, 45 (2008) 581-595.

[7] S. Banerjee, T. Kundu, Elastic wave propagation in sinusoidally corrugated waveguides, The Journal of the Acoustical Society of America, 119 (2006).

[8] S. Das, C.M. Dao, S. Banerjee, T. Kundu, DPSM modeling for studying interaction between bounded ultrasonic beams and corrugated plates with experimental verification, ieee transactions on ultrasonics, ferroelectrics, and frequency control, 54 (2007) 1860-1872.

[9] T. Hajzargarbashi, E.K. Rahani, T. Kundu, Scattering of focused ultrasonic beams by two spherical cavities in close proximity, IEEE transactions on ultrasonics, ferroelectrics, and frequency control, 58 (2011) 1619-1627.

[10] T. Kundu, J.-P. Lee, C. Blase, J. Bereiter-Hahn, Acoustic microscope lens modeling and its application in determining biological cell properties from single-and multi-layered cell models, The Journal of the Acoustical Society of America, 120 (2006) 1646-1654.

[11] S. Fooladi, T. Kundu, Ultrasonic field modeling in anisotropic materials by distributed point source method, Ultrasonics, 78 (2017) 115-124.

[12] T. Kundu, D. Placko, E.K. Rahani, T. Yanagita, C.M. Dao, Ultrasonic field modeling: A comparison of analytical, semi-analytical, and numerical techniques, IEEE transactions on ultrasonics, ferroelectrics, and frequency control, 57 (2010) 2795-2807.
[13] T. Bore, D. Placko, F. Taillade, P. Sabouroux, Electromagnetic characterization of grouting materials of bridge post tensioned ducts for NDT using capacitive probe, NDT & E International, 60 (2013) 110-120.
[14] S. Banerjee, T. Kundu, N.A. Alnuaimi, DPSM technique for ultrasonic field modelling near fluid–solid interface, Ultrasonics, 46 (2007) 235-250.
[15] A. Shelke, S. Das, T. Kundu, Distributed point source method for modeling scattered ultrasonic fields in the presence of an elliptical cavity, Structural health monitoring, 9 (2010) 527-539.
[16] S. Fooladi, T. Kundu, Distributed point source modeling of the scattering of elastic waves by a circular cavity in an anisotropic half-space, Ultrasonics, 94 (2019) 264-280.
[17] A.J. Jarvis, F.B. Cegla, Scattering of near normal incidence SH waves by sinusoidal and rough surfaces in 3-D: Comparison to the scalar wave approximation, IEEE Transactions on Ultrasonics, Ferroelectrics, and Frequency Control, 61 (2014) 1179-1190.
[18] P. Kot, M. Muradov, M. Gkantou, G.S. Kamaris, K. Hashim, D. Yeboah, Recent advancements in non-destructive testing techniques for structural health monitoring, Applied Sciences, 11 (2021) 2750.
[19] W. Dong, Y. Huang, B. Lehane, G. Ma, An artificial intelligence-based conductivity prediction and feature analysis of carbon fiber reinforced cementitious composite for non-destructive structural health monitoring, Engineering Structures, 266 (2022) 114578.
[20] F. Dipietrangelo, F. Nicassio, G. Scarselli, Structural Health Monitoring for impact localisation via machine learning, Mechanical Systems and Signal Processing, 183 (2023) 109621.
[21] N.M. Kalimullah, A. Shelke, A. Habib, A deep learning approach for anomaly identification in PZT sensors using point contact method, Smart Materials and Structures, 32 (2023) 095027.
[22] K. Hornik, M. Stinchcombe, H. White, Universal approximation of an unknown mapping and its derivatives using multilayer feedforward networks, Neural networks, 3 (1990) 551-560.
[23] G. Gybenko, Approximation by superposition of sigmoidal functions, Mathematics of Control, Signals and Systems, 2 (1989) 303-314.

[24] T. Gantala, K. Balasubramaniam, DPAI: A Data-driven simulation-assisted-Physics learned AI model for transient ultrasonic wave propagation, Ultrasonics, 121 (2022) 106671.
[25] T. Fu, Z. Zhang, Y. Liu, J. Leng, Development of an artificial neural network for source localization using a fiber optic acoustic emission sensor array, Structural Health Monitoring, 14 (2015) 168-177.
[26] S. Kalafat, M.G. Sause, Acoustic emission source localization by artificial neural networks, Structural Health Monitoring, 14 (2015) 633-647.
[27] M. Raissi, P. Perdikaris, G.E. Karniadakis, Physics-informed neural networks: A deep learning framework for solving forward and inverse problems involving nonlinear partial differential equations, Journal of Computational physics, 378 (2019) 686-707.
[28] S. Goswami, C. Anitescu, S. Chakraborty, T. Rabczuk, Transfer learning enhanced physics informed neural network for phase-field modeling of fracture, Theoretical and Applied Fracture Mechanics, 106 (2020) 102447.
[29] E. Haghighat, M. Raissi, A. Moure, H. Gomez, R. Juanes, A physics-informed deep learning framework for inversion and surrogate modeling in solid mechanics, Computer Methods in Applied Mechanics and Engineering, 379 (2021) 113741.
[30] F.A. Viana, R.G. Nascimento, A. Dourado, Y.A. Yucesan, Estimating model inadequacy in ordinary differential equations with physics-informed neural networks, Computers & Structures, 245 (2021) 106458.
[31] K. Shukla, P.C. Di Leoni, J. Blackshire, D. Sparkman, G.E. Karniadakis, Physics-informed neural network for ultrasound nondestructive quantification of surface breaking cracks, Journal of Nondestructive Evaluation, 39 (2020) 1-20.
[32] H. Wang, J. Li, L. Wang, L. Liang, Z. Zeng, Y. Liu, On acoustic fields of complex scatters based on physics-informed neural networks, Ultrasonics, 128 (2023) 106872.
[33] L. Lu, P. Jin, G.E. Karniadakis, Deeponet: Learning nonlinear operators for identifying differential equations based on the universal approximation theorem of operators, arXiv preprint arXiv:1910.03193, (2019).
[34] G. Lin, F. Chen, P. Hu, X. Chen, J. Chen, J. Wang, Z. Shi, BI-GreenNet: learning Green's functions by boundary integral network, Communications in Mathematics and Statistics, 11 (2023) 103-129.
[35] L. Zhang, T. Luo, Y. Zhang, Z.-Q.J. Xu, Z. Ma, MOD-Net: A machine learning approach via model-operator-data network for solving PDEs, arXiv preprint arXiv:2107.03673, (2021).
[36] A.K. Mal, S.J. Singh, Deformation of elastic solids, Prentice Hall New Jersey, 1991.

[37] S. Das, T. Kundu, Mesh-free modeling of ultrasonic wave fields in damaged layered half-spaces, Structural Health Monitoring, 8 (2009) 369-379.
[38] T. Kundu, D. Placko, DPSM for modeling engineering problems, John Wiley & Sons, 2007.
[39] K. Hornik, M. Stinchcombe, H. White, Multilayer feedforward networks are universal approximators, Neural networks, 2 (1989) 359-366.
[40] C.M. Bishop, N.M. Nasrabadi, Pattern recognition and machine learning, Springer, 2006.
[41] C.C. Aggarwal, Neural networks and deep learning, Springer, 10 (2018) 3.
[42] I. Goodfellow, Y. Bengio, A. Courville, Deep learning, MIT press, 2016.
[43] G.E. Karniadakis, I.G. Kevrekidis, L. Lu, P. Perdikaris, S. Wang, L. Yang, Physics-informed machine learning, Nature Reviews Physics, 3 (2021) 422-440.
[44] S. Das, S. Banerjee, T. Kundu, Elastic wave scattering in a solid half-space with a circular cylindrical hole using the Distributed Point Source Method, International journal of solids and structures, 45 (2008) 4498-4508.
[45] S. Cai, Z. Wang, S. Wang, P. Perdikaris, G.E. Karniadakis, Physics-informed neural networks for heat transfer problems, Journal of Heat Transfer, 143 (2021) 060801.
[46] X. Meng, G.E. Karniadakis, A composite neural network that learns from multi-fidelity data: Application to function approximation and inverse PDE problems, Journal of Computational Physics, 401 (2020) 109020.
[47] N.M.-M. Kalimullah, A. Shelke, A. Habib, A probabilistic framework for source localization in anisotropic composite using transfer learning based multi-fidelity physics informed neural network (mfPINN), Mechanical Systems and Signal Processing, 197 (2023) 110360.
[48] J. Snoek, H. Larochelle, R.P. Adams, Practical bayesian optimization of machine learning algorithms, Advances in neural information processing systems, 25 (2012).
[49] D. Placko, T. Kundu, Theoretical study of magnetic and ultrasonic sensors: dependence of magnetic potential and acoustic pressure on the sensor geometry, in: Advanced Nondestructive Evaluation for Structural and Biological Health Monitoring, SPIE, 2001, pp. 52-62.
[50] D. Placko, T. Kundu, R. Ahmad, Theoretical computation of acoustic pressure generated by ultrasonic sensors in the presence of an interface, in: Smart Nondestructive Evaluation for Health Monitoring of Structural and Biological Systems, SPIE, 2002, pp. 157-168.

[51] T. Kundu, Ultrasonic nondestructive evaluation: engineering and biological material characterization, CRC press, 2003.
[52] D. Placko, N. Liebeaux, T. Kundu, D. Balageas, Presentation d'une method generique pour la modelisation des capteurs de type ultrasons, Magnetiques at Electrostatiques, Instrumentation, Mesure, Metrologie (I2M Journal): Evaluation Nondestructive, 1 (2001) 101-125.